Available online at www.sciencedirect.com
ScienceDirect
Marine Structures 20 (2007) 218–237
MARINE STRUCTURES
www.elsevier.com/locate/marstruc

On the resistance of tanker bottom structures during stranding

Hagbart S. Alsos*, Jørgen Amdahl

Department of Marine Technology, Norwegian University of Science and Technology, Otto Nielsens V. 10, 7491 Trondheim, Norway

Received 24 April 2007; accepted 7 June 2007

Abstract

The paper deals with grounding and stranding of ships. An important issue is the influence of size and shape of the sea floor during grounding. From a range of finite element simulations, the resistance to penetration of the ship bottom is found, for stranding at various locations and different sea bottom topologies.

A description of the state of the art material and failure methods is given, and the theory is applied in finite element analyses. Furthermore, a mesh convergence study is carried out in order to find the appropriate mesh for the grounding simulations.

Integrated local/global grounding analyses are performed. Stranded ships may be subjected to tidal changes, which may result in further bottom damage. The loss in water level yields a re-distribution of hydrostatic forces due to grounding actions. In this process large hull bending moments are formed, which may influence the resistance to penetration and the damage modes significantly.

Keywords: Grounding; Stranding; Crushing; Penetration; Fracture; Hull resistance; Global response

1. Introduction

Historical and recent events have made it clear that ship grounding and collision represent significant hazards. This applies both with respect to loss of human lives, severe environmental consequences and economical loss. The most typical consequence of ship

*Corresponding author. Tel.: +47 735 50446; fax: +47 735 95697.
E-mail addresses: hagbarts@ntnu.no (H.S. Alsos), jorgen.amdahl@ntnu.no (J. Amdahl).
URL: http://folk.ntnu.no/hagbarts (H.S. Alsos).

0951-8339/$ - see front matter © 2007 Elsevier Ltd. All rights reserved.
doi:10.1016/j.marstruc.2007.06.001

grounding and collision is oil spill, as exemplified for instance by the Sea Empress which spilled 65,000 ton of crude oil at Milford Haven harbor, Wales, in 1996. In 1997, the Nakhodka, a Russian tanker carrying 19,000 ton of heavy fuel oil broke in two during storms in the Sea of Japan with severe environmental consequences. On the Norwegian coast several accidents have occurred that have caused serious public concern. In 1992 the Panama registered bulk carrier "Arisan" grounded near the famous bird nesting cliff Runde and considerable amounts of oil were threatening the island. In the fall of 2000, "Green Ålesund" capsized close to Haugesund and "John R" stranded and broke into two on Grøtøy North of Tromsø. In both cases, only favorable weather conditions prevented major oil pollution. A recent high profile accident is the sinking of the oil tanker Prestige off the Spanish coast. These events demonstrates that the risk level is not acceptable, and that public awareness of sub-standard transportation systems is increasing. The risk of massive spill or casualties constitutes a threat to sustainable development. Improvement of casualty prevention measures is, therefore, essential to obtain the desired level of safety at sea and protection of marine ecosystems.

In response of the significant risk of marine accidents, a joint industry project supported by the European Community was launched in 2004. The project is entitled decision support system for ships in degraded condition "DSS_DC". The aim of the project is to establish an emergency assistance system for ships in critical situations. Based on communication with an on shore unit and an established databases on the structural and hydrodynamic properties, advice can be given to ship masters on actions to be taken. Examples are to de-ballast cargo for bending moment relaxation, or to outline favorable sailing directions to reduce sea loads, if the ship has suffered critical damage in open waters. If actions are not taken, the worst outcome may be a vessel breaking into two and sinking. The Prestige accident demonstrated that ship wrecks potentially may leak oil for years, thereby representing a continuous pollution threat. Hence, a last resort in a critical situation may be to run the ship aground in sheltered waters, allowing e.g. for safe discharging of oil. However, running the ship aground is by itself a risky undertaking. At present, very few tools are available to the relevant decision makers to assess the consequences of such a decision.

The purpose of the paper is to study the response and resistance of stranded ships. A parametric study of sea floor topology and the structural damage this causes at grounding is performed. Furthermore global effects from tidal changes are also investigated. In the simulation process, a user defined version of the finite element (FE) code LS-DYNA is applied. This allows for better material and rupture control. Finally, to confirm the accuracy of the ship model, a mesh convergence study is undertaken.

2. Bottom topology and grounding scenarios

Ship grounding is a very complex process. It involves large contact forces, crushing of hull structure, rupture of shell plating, all while interacting with global motions. The consequences may be severe and the process is highly nonlinear. The property of the sea bed is one of the governing factors within the damage process. Adequate information on sea floor topology is, however, very limited. Analyses typically adopt ideas and assumptions made in previously published work. Apparently many of these seem to originate from high profile accidents. An example is the Exxon Valdez grounding in Alaska 1989, where a pinnacle opened a large part of the ships bottom plating. Wierzbicki et al.

[1,2] adopted these damage patterns, and have developed analytical closed form solutions for cutting mechanisms. Simonsen [3,4] has taken this further in the search for analytical expressions for raking problems. This theory has further been implemented into the grounding analysis code DAMAGE [5], by Wierzbicki and his colleagues at MIT.

In stranding analysis focus has mostly been placed on penetration and crushing mechanisms. This resembles the collision problem in the sense that a truncated cone is forced through and puncture the hull plating, see e.g. Amdahl et al. [6], Naar et al. [7]. The effect of different indenter shape and size has been investigated by Wang et al. [8]. This was done through a series of scaled down double bottom grounding experiments. The study clearly shows that small indenters puncture the hull skin with relative ease, while larger indenters damage the internal web configuration before the shell plating ruptures. Wang et al.'s [8] work is clearly a step forward in the field of collision and grounding. However, in order to better understand the interaction between the ship hull and the sea bed during grounding, further studies and analyses are needed.

In order to better predict damage and ship response during grounding, a survey of actual sea floor topologies in navigation channels may prove useful. This could, e.g. be carried out in critical waters where grounding is likely to take place, or at potential stranding sites. At present, such data are merely non-existing. Another potential source of sea floor geometry may be found from reports on grounding damage. IMO launched in 2000 the HARDER project, which was concluded in May 2003. The purpose of this project was to develop a concept of probabilistic damage stability for ships. Within this work, data on collision and grounding damage was collected, which formed the basis for a damage database. This project and other ongoing programs on marine accidents are further described in the 2006 ISSC collision and grounding report [18]. The damage data from the HARDER database has been processed by Lützen et al. [9]. This has resulted in various statistical distributions for different types of collision and grounding scenarios. An interesting, but perhaps obvious relation is shown in Fig. 1. Even though the datapoints

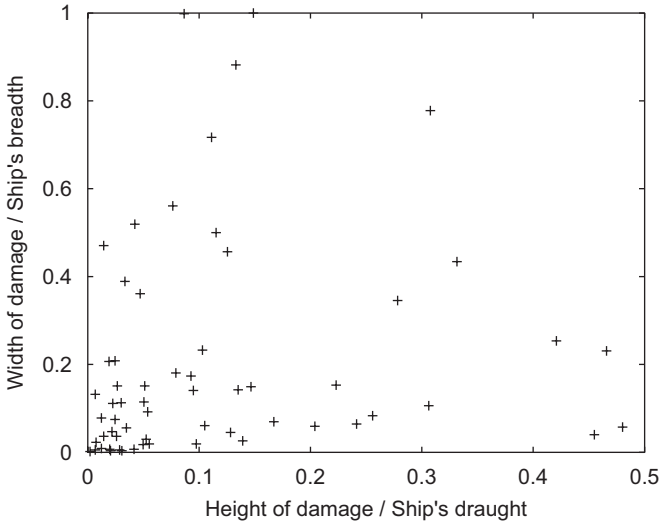

Fig. 1. Sampled data from the IMO HARDER project [9].

are scattered, trends can be found. If deformations go deep into the hull, the magnitude of structural damage is likely to be local. If, on the other hand, large parts of the ship breadth is damaged, the penetration will be small. In other words, the difference in structural damage can to some extent be attributed to the shape and size of the obstruction on the sea floor.

Based on the extent of damage, it is possible to establish a set of indenters which may represent the seafloor obstruction. In the following, three indenter topologies are presented:

(1) "*Rock*": Indenters much smaller than the ship itself, such as the "rock", are expected to create local damage, e.g. hull puncturing while the overall structure remains intact. Pinnacles and truncated cones, Simonsen [3] and Amdahl [6,10], fall under this category. In the present work, the "rock" takes shape of a paraboloid with a bottom diameter of $0.2B$, where B is the ship beam.
(2) "*Shoal*": The "shoal" represents a very different indenter type. By contrast to the "rock", the surface of the "shoal" is relatively large. In the following studies, the "shoal" dimension is about half the ships hull width. Large parts of the hull are expected to be damaged during "shoal" grounding.
(3) "*Reef*": The "rock" and "shoal" describe two very different indenters. An intermediate indenter is therefore established, referred to as "reef". In this case it is not so easy to see the response of the double bottom in terms of local or global deformations à priori.

In addition to indenter shape and size, friction properties also affect the response. Typically, static coulomb friction coefficients in the range of 0.2–0.4 are adopted for steel to steel and steel to rock contact, see for example [1–3]. However this may vary significantly, depending on lubricating effects from marine growth, oil spill or surface roughness. Zhang [11] investigated the effects of friction in a series of raking analyses and found a great difference in force levels for coefficients varying below 0.3. However, bottom raking is mostly a cutting process and is very different from quasi static crushing and penetration processes. In static grounding the work is conducted normal to the structure's surface. Hence, the friction effect is expected to be weak. In the simulations carried out in the following sections, the standard value of 0.3 has been adopted.

3. Ship model

Stranding simulations are performed for various penetration scenarios with the explicit FE code LS-DYNA. The ship considered is a 260 m shuttle tanker with a double bottom configuration, Fig. 2. The width of the ship is 42 m, mean draught 15 m, and the average tank length is 32 m.

3.1. Grounding scenarios

The three indenters shown in Fig. 2 are applied at four different locations as indicated in Fig. 3. Location 1, represents contact in the middle of a cargo tank. Location 2, implies crushing of the transverse bulkhead, away from the longitudinal center line. Location 3 considers grounding in the middle of the tank section, at the longitudinal center line.

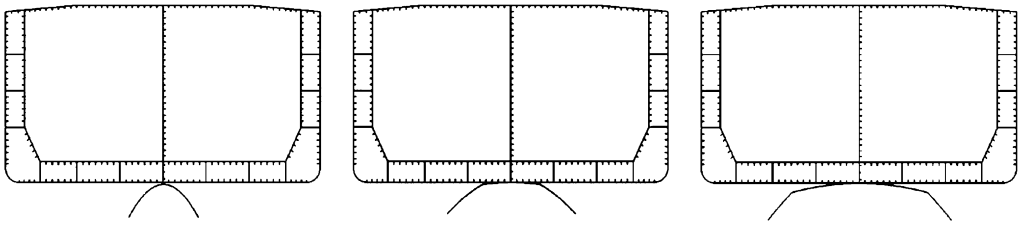

Fig. 2. Sea bed conditions: (a) "rock"; (b) "reef"; (c) "shoal".

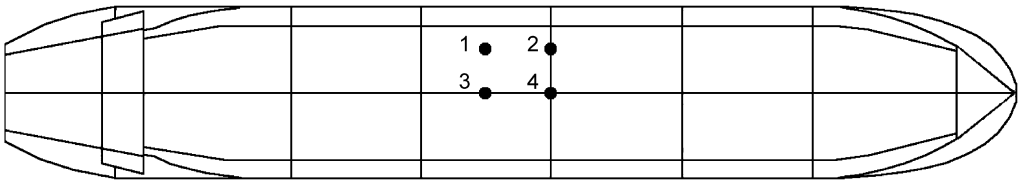

Fig. 3. General arrangement. The bullets highlight the positions of the indenters.

The same goes for location 4, but rather than crushing the mid tank, the action is taking place at the transverse bulkhead. In total, this gives 12 scenarios (four scenarios for each indenter).

3.2. Structural arrangement

To avoid interference with boundaries, the ship model spans over almost two tank lengths. This yields a rather big structural system, which sets limitations to the mesh fineness. Zones subjected to little deformations are more coarsely meshed than areas subjected to large deformations. This limits the simulation time while maintaining the accuracy. The mesh size is determined from convergence tests, presented in Section 4. The element of choice is the one point quadrature Belytschko–Tsay element, which is both accurate and effective, e.g. [11,12]. Contact is accounted for by the general automatic contact options found in LS-DYNA. The boundaries of the tank beam sections follow the properties of a Bernoulli beam, i.e. plane cross-sections remain plane. This means that the model ends are allowed to rotate freely about the neutral axis. The model is displayed in Fig. 4.

3.3. Material and fracture

Two steel grades are represented over the cross-section, the mild steel and the higher strength A-36 steel. The plastic properties of these steel qualities may be described by the power law

$$\sigma = C(\bar{\varepsilon} + \varepsilon_0)^n, \tag{1}$$

where $\bar{\varepsilon}$ is the effective plastic strain, (C, n) are material parameters, and ε_0 describes the initial state, $\varepsilon_0 = \sqrt[n]{\sigma_Y/C}$, given by the yield stress σ_Y. The power-law parameters are given in Table 1.

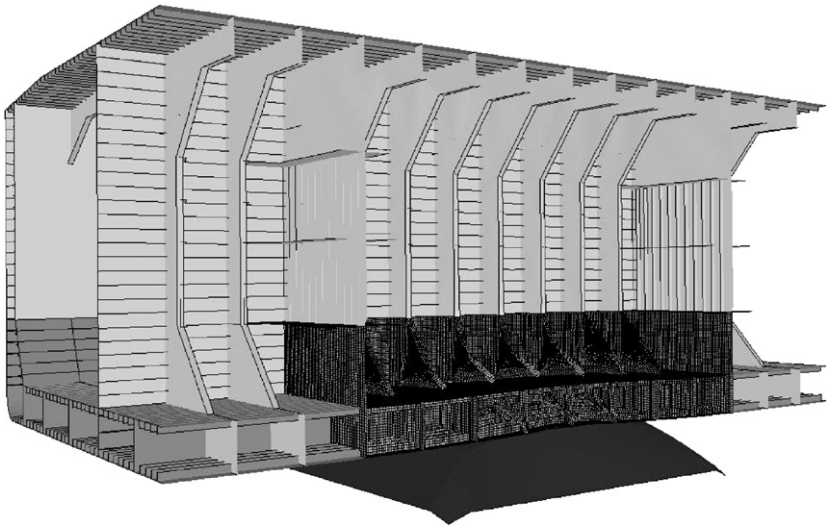

Fig. 4. FE model of the ship. The model is opened to show the inner configuration.

Table 1
Power-law material parameters

Material	σ_Y (MPa)	C (MPa)	n (–)
Mild steel	225	670	0.25
A-36 steel	370	750	0.2

Correct prediction of rupture is a key factor in crashworthiness analysis. The magnitude of deformation before fracture varies with the quality of the steel and the stress state involved. The stress state, often referred to as the stress triaxiality, is defined by the hydrostatic stress, σ_m, over the equivalent von Mises stress, σ_{eq}, i.e. $T = \sigma_m/\sigma_{\text{eq}}$. The hydrostatic stress, σ_m, is independent of shear components, while the von Mises stress, σ_{eq}, is pressure independent. This makes the stress triaxiality, T, able to describe the full range of stress states as a single variable, which is very convenient.

Triaxialities above $\frac{1}{3}$, describe tension stress states. On a micro-structural level, fracture is driven by small impurities inside the material which nucleates and creates material voids. As the deformation continues, these voids grows and coalesces. Fracture takes place when the ligament between the voids have thinned down to a certain level. Stress triaxialities below $-\frac{1}{3}$, describe a compression state. As a general, fracture will not initiate in this state. Between the compression and tension, fracture appears in a shear state.

There are several fracture models available to simulate rupture. Most of them adopt damage criteria to either describe shear damage or void growth. Many of them are, however, too complex for practical use. The default approach followed by most engineers today is failure at some critical equivalent strain. It is simple and incorporated method in most nonlinear FE codes. The disadvantage with this criterion is the complete neglection of the stress triaxiality, Fig. 5. It shows constant ductility for all variations of stress

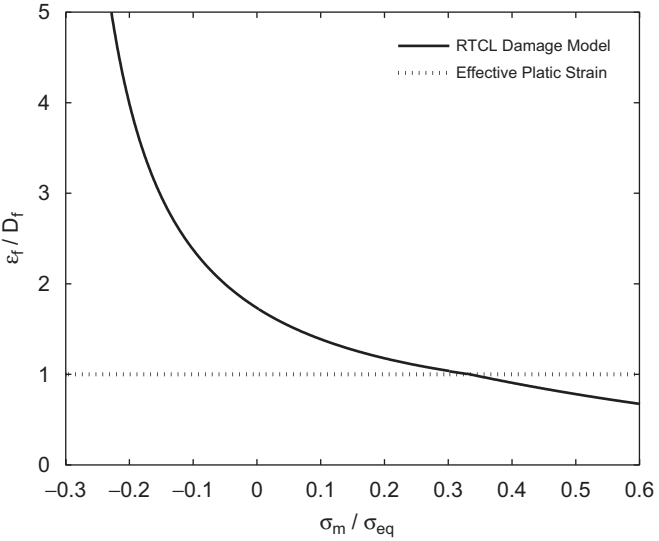

Fig. 5. Failure strain response normalized by the critical damage. Curves are made for both the RTCL damage criterion and the equivalent plastic strain criterion, as functions of the stress triaxiality.

triaxiality, and may even yield fracture in pure compression. This is unphysical. Therefore, a damage approach in the form of the RTCL criterion is adopted. This model applies the combination of the Cockcroft–Latham damage model [13] and Rice–Tracey void growth criterion [14]. Together they cover the full stress triaxiality range, and have been extensively verified by Törnqvist at DTU [15,16]. The expression yields

$$D = \begin{cases} \int \frac{\sigma_1}{\sigma_{eq}} \, d\varepsilon_{eq} & \text{if } -\frac{1}{3} \leqslant T \leqslant \frac{1}{3}, \\ \int \frac{1}{C} \exp(\frac{3}{2} T) \, d\varepsilon_{eq} & \text{if } \frac{1}{3} \leqslant T, \end{cases} \tag{2}$$

where D is the accumulated damage, $d\varepsilon_{eq}$ is the effective plastic strain increment, and T is the stress triaxiality. The criterion is compared with the effective strain criterion in Fig. 5. Törnqvist has shown [14] that the RTCL model behaves well for $C = 1.65$, which is convenient with respect to calibration. At $T = 0.33$, the damage value and effective strain intersect, such that calibration can be made with one single tensile test, see Fig. 5.

Structural elements and especially shells are very mesh size sensitive close to fracture. Due to high strain gradients, failure will have to take place at different damage levels for different mesh sizes. In order to achieve true convergence, mesh refinement and nonlocal methods (for shells) need to be applied. This is, however, not applicable in large scale ship analysis. Another and simplified mesh handling option is found from mesh sensitivity curves [16], as in Fig. 6. These assumes a relation between critical damage and element size. This relation can be found from simulation of a tensile test until fracture, with different mesh sizes. Fracture will then appear at different damage values for each mesh configuration. In reality, this means that the effect of strain gradients in diffuse and local necks are assumed similar to strain gradients along discontinuous details, such as crack surfaces. The method is not entirely consistent, but it is able to provide reasonable prediction of the critical damage value according to the element size. The mesh-damage

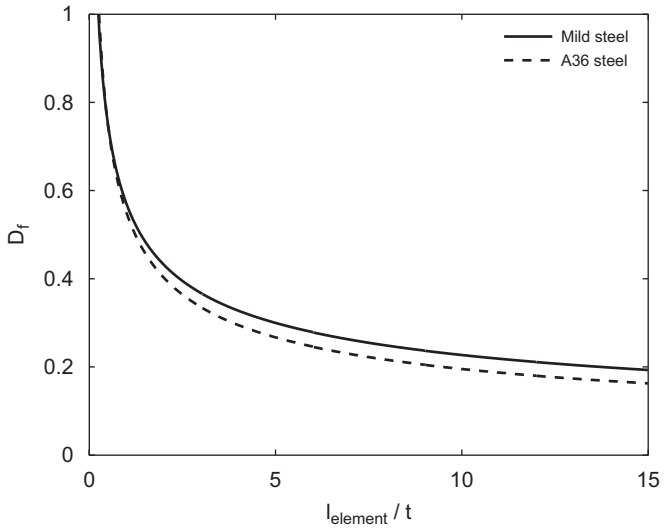

Fig. 6. RTCL damage scaling. The scaling is a function of the element size.

relation is implemented into LS-DYNA. In the user defined version, it automatically reads the element size and thickness and outputs the according critical damage value.

4. Mesh convergence study

Many studies on grounding and collision are carried out with relatively coarse finite element (FE) meshes and limited information on mesh behavior. This leaves uncertainties to the accuracy of the analyses. Ideally, FE models should be made as accurate and detailed as possible in order to capture local folding and instability effects. This may require excessive computational time and resources. On the other hand, fast simulations with coarse meshes may satisfy the requirements to computational efficiency, but may fail to meet accuracy requirements. Convergence analysis should therefore be conducted to determine the point where both computational costs and accuracy can be justified. This should preferably be carried out on highly deformed and major structural members, e.g. the double bottom girder–floor intersection in grounding studies.

The girder intersection selected for the convergence study constitutes a cruciform, as shown in Fig. 8. Due to the regularity of the bottom structure, the four edges of the cruciform are given symmetry conditions. The cruciform is 2680 mm high, with girder length 4000 mm, floor width 5800 mm, and plate thickness 15 mm. Secondary, sniped vertical stiffeners are applied to the floors (transverse-girders), while the longitudinal girder has longitudinal stiffeners. In order to investigate the importance of the cruciform stiffening, the case without stiffeners is also studied. Both the stiffened and unstiffened configuration is analyzed with four mesh sizes. All models are represented by Belytschko–Tsay shell elements [17] with five integration points through the thickness, in order to simulate bending decently. Other element types are also investigated, but very little difference is observed. In the following convergence tests, the mesh size is characterized by the number of elements over the cruciform height, ranging from the coarse 6 element mesh, 6-el, to the

fine 24 element mesh, 24-el. The study is purely on deformation-load convergence, hence the effect of fracture is left out.

The difference in energy between including and disregarding stiffeners is shown in Fig. 7(a) and (b). As expected, the energy level rises when stiffening is included. It is interesting to see that mesh convergence appears faster for the stiffened than the unstiffened cruciform. This is explained by the fact that stiffeners increases the folding wave length. Convergence is achieved by the 18-el mesh, but the trend is already pronounced by the 12-el mesh. When secondary stiffeners are omitted, convergence is slowed down because of the increased number of folding waves close to the cruciform intersection, as the mesh is refined. The 18-el mesh with stiffeners included is therefore used in the large ship model. This yields an element size close to 150 mm, which is on the average less than 10 times the shell thickness. This may seem rather coarse, but the total model contains about 600000 elements, which is quite CPU demanding.

A simple way to avoid modeling of secondary stiffeners goes through thickness smearing of stiffeners. This may either be based on the plastic section modulus or the cross-section

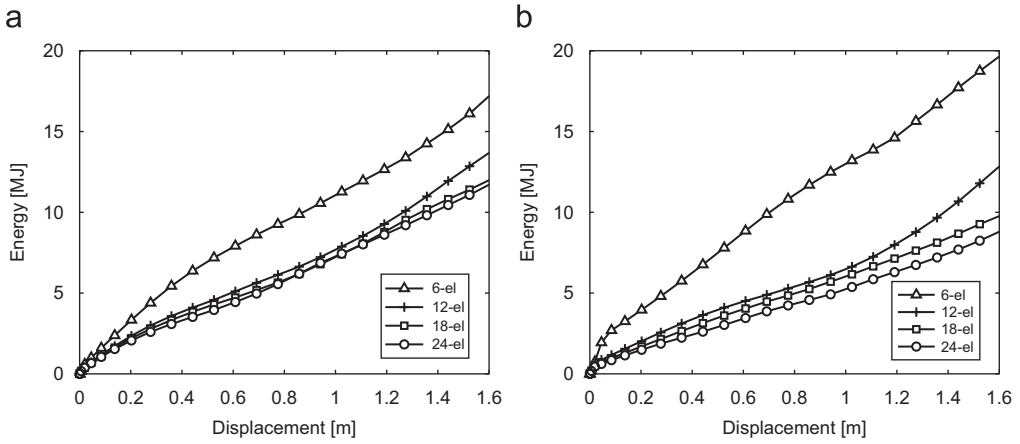

Fig. 7. Internal energy convergence: (a) stiffened cruciforms; (b) nonstiffened cruciforms.

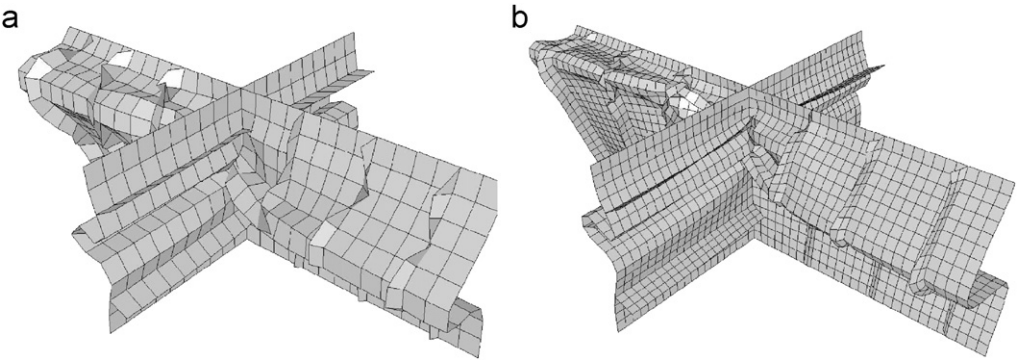

Fig. 8. Mesh convergence study. The two stiffened models represents: (a) the 12-el mesh; and (b) the denser 24-el mesh.

area, depending on whether the governing response is bending or axial membrane. However, smearing displays the same convergence drawbacks as the non-stiffened cruciform. The simplicity in modeling yields more elements to maintain accuracy. Furthermore, smearing does not account for orthotropy of the stiffened web. Thus, the method requires careful judgment and awareness of expected deformations. In addition, the fracture properties are significantly altered. Not only is the plate thickness changed, but also the crack growth constraints imposed by the stiffeners. In the end, there is little to gain by applying smearing techniques.

5. Structural resistance at grounding

This section describes the structural response of the tanker when subjected to grounding actions. The focus is purely on the double bottom resistance during grounding. Other effects such as global ship motions have therefore not been considered. All simulations are carried out as outlined in Section 3.

5.1. Rock resistance

Fig. 9 illustrates the typical deformation response of the ship when stranding on a "rock". The indenter penetrates the outer and inner shell plating and crushes web structure. The damage is local, and affects only structural members in the close proximity of the "rock". The similarity with the structural response in ship collisions is obvious.

Fig. 10(a) illustrates the resistance for the various "rock" scenarios. Inspection of the curves show that a significant part of the contact forces are initially carried by membrane stresses in the shell plating. Once the outer plating ruptures, the resistance falls dramatically. Depending on the indenter position, the loss of resistance may be as much as 50%. The difference in fracture point appears to be insignificant when considering the total penetration. However, there is a distinct pattern in where and when failure occurs. Grounding on stiff structural parts such as bulkhead intersections (scenario 4) shows earlier fracture than grounding at the weaker girder–floor intersection, e.g. scenario 1. The reason is that weaker sections are not able to carry the grounding load. Damage is therefore spread out over larger zones. Stiff sections, on the other hand, can sustain these loads and are therefore only damaged locally. Rupture is therefore observed at a slightly earlier stage when grounding takes place on stiff parts than at weaker locations. The same effect is reported by Naar et al. [7] who studied the resistance of various double bottom structures during "rock" type penetration.

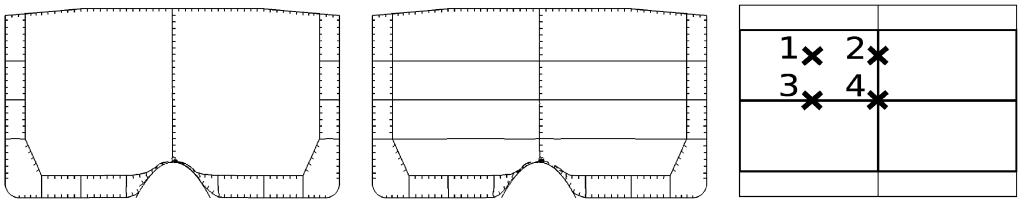

Fig. 9. Left, cross-section deformation in mid tank (scenario 3). Middle, cross-section deformation at transverse bulkhead (scenario 4). Right, scenario contact points.

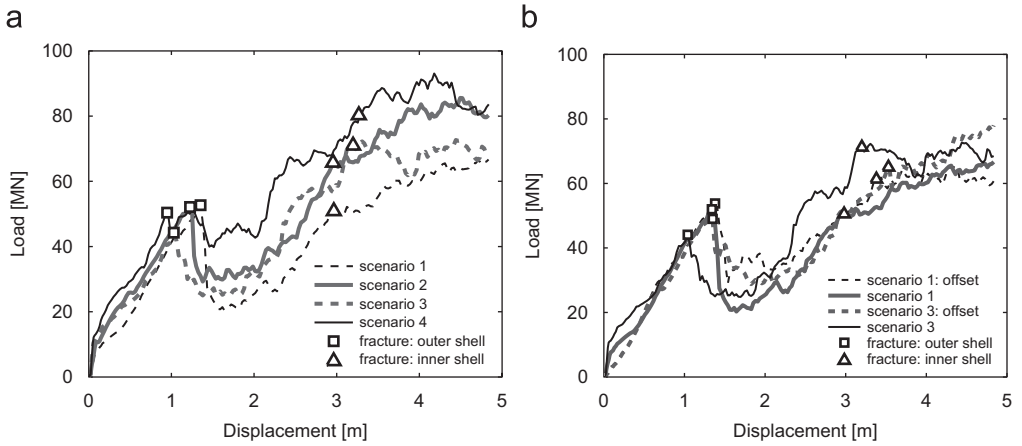

Fig. 10. Force deformation plots for rock penetration. Curves in (a) shows ordinary rock scenarios 1–4; (b) compares ordinary scenarios with offset scenarios.

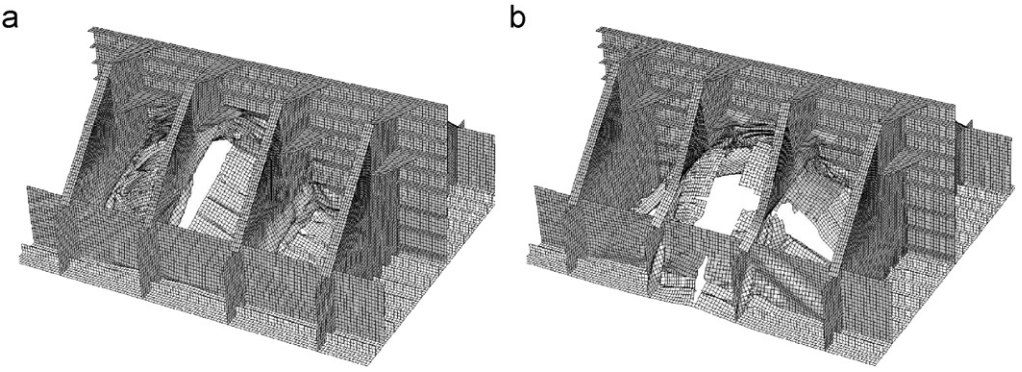

Fig. 11. Crushing modes: (a) crushing at longitudinal bulkhead (scenario 3); (b) grounding between floors, longitudinal bulkhead and girders (offset scenario 3).

The response after first rupture, varies considerably. With the loss of membrane carrying capacity in the outer skin, the remaining resistance is found in the web and inner bottom plating. Hence, grounding on relatively weak girder floor configurations, as in scenario 1 yields less resistance than the stronger bulkhead intersection in scenario 4.

For evaluation of the ''rock'' scenarios, two additional analyses are performed. The difference from the previous four scenarios is the new position of the ''rock''. Rather than crushing directly on vertical members such as girders, floors and bulkheads, the indenter is located between the web. Contact is therefore carried only through the shell plating. Except from the offset location of the indenter, the additional analyses, ''offset scenario 1 and 3'', are equivalent to the ''original scenarios 1 and 3''. The forces from these are compared in Fig. 10(b). Before fracture, there is little difference in force levels. At this stage, the membrane actions predominate the response. First fracture appears for the same penetration as in ''rock'' scenario 1. The kinematic response in both original and offset

scenarios is shown in Fig. 11. Contrary to the original scenarios which are subjected to web crushing before and after bottom plate rupture, the web structure in the "offset scenarios 1 and 3" are torn apart after the hull skin rupture. Since the web tearing modes are very similar for both of the offset scenarios, the resistance curves follow almost the same curve path.

5.2. Shoal resistance

Contrary to the puncturing effect of the "rock", the large "shoal" causes wide spread bottom damage, as Fig. 12 shows. The slightly curved "shoal" surface initiates crushing of the web once contact is established. Crushing is the main deformation mechanism in the contact zone, and areas around bulkheads. Some distance away from the contact point, the web is subjected to grillage deformation. At approx. 1.7 m penetration, the bulkhead structure fails above the inner bottom, and starts folding, Fig. 12. This changes the deformation pattern in the double bottom from a mixture of crushing and grillage deformation to predominant grillage deformation. After approximately 3 m indenter displacement, the

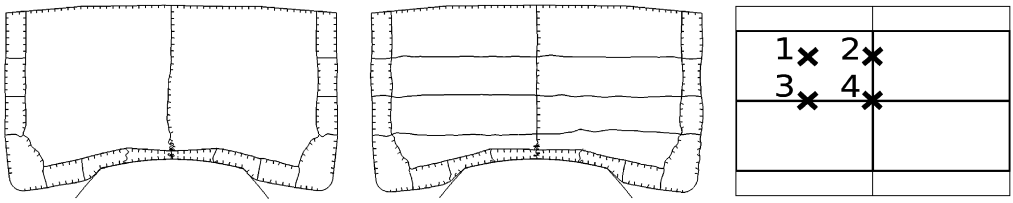

Fig. 12. Left, cross-section deformation in mid tank (scenario 3). Middle, cross-section deformation at transverse bulkhead (scenario 4). Right, scenario contact points.

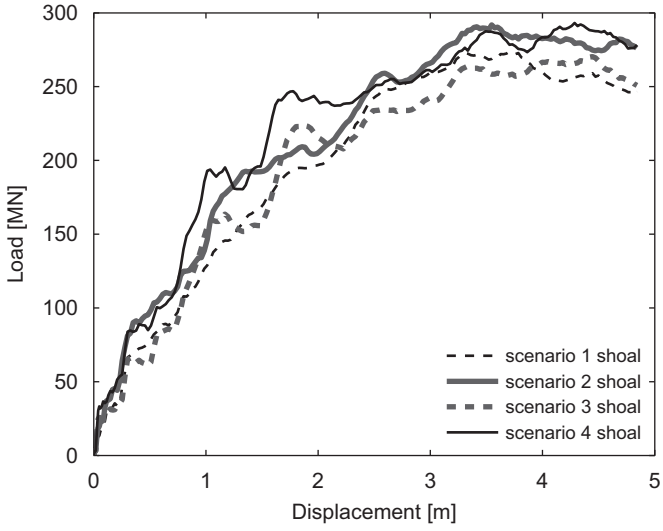

Fig. 13. Force deformation plots for shoal penetration.

cross-section reaches its maximum resistance. The hull starts breaking up, followed up by rotation of both parts of the hull.

Fig. 13 shows the resistance curves for the four scenarios. The surface of the indenter is so large that the contact location is of minor importance, with respect to finding a resistance curve. It is, however, interesting to observe the behavior of scenarios 2 and 4, Fig. 13, which represent stranding on the transverse bulkhead. The pronounced stepwise increase of resistance is due to sequential buckling and folding of the vertically stiffened transverse bulkhead. The longitudinal bulkhead, which is stiffened horizontally, does not exhibit this response.

5.3. Reef resistance

Bottom damage due to "reef" grounding is illustrated in Fig. 14. The response is clearly influenced by the position of the indenter. Crushing at the transverse bulkhead, Fig. 14(b), causes predominantly local damage, similar to stranding on a "rock". Crushing the side tanks (scenario 1 and 2) yield the same response due to support from side and bulkheads. Grounding at mid tank, on the other hand, Fig. 14(a), results in global damage.

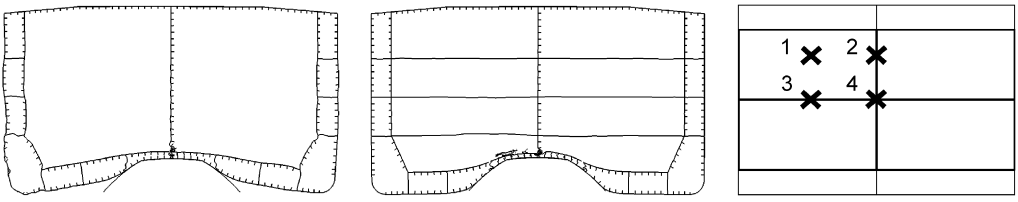

Fig. 14. Left, cross-section deformation in mid tank (scenario 3). Middle, cross-section deformation at transverse bulkhead (scenario 4). Right, scenario contact points.

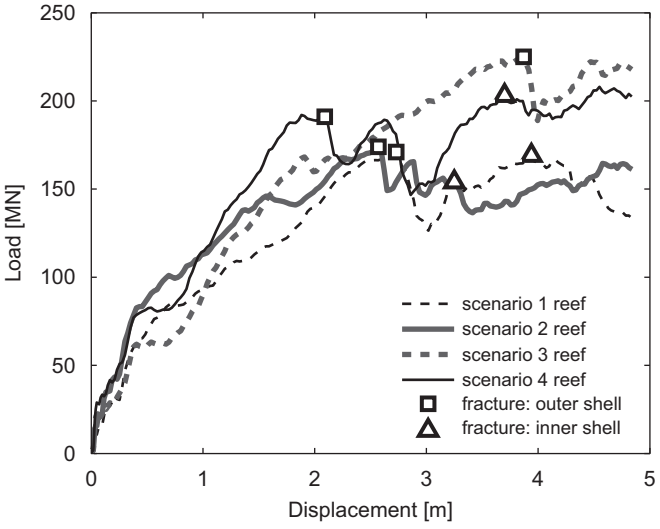

Fig. 15. Force deformation plots for reef penetration.

As for shoal grounding, the damage modes are governed by combined crushing and grillage deformation. The response is confirmed by the late rupture in the inner and outer shell, see Fig. 15.

It is interesting to observe that the "reef" indenter truely captures an intersection point between local and global damage. Moreover, it adds another aspect to possible crashworthiness design. For example, in order to reduce the likelihood of hull rupture, the internal structural configuration may be made relatively weak. Deformations will then be spread out over large zones and cause little strain localizations in the hull plating. On the other hand, this may also weaken the ships resistance with respect to hull girder collapse.

6. Interaction with bending moments

Large forces are involved during grounding. It was shown in Section 5 that the actions at stranding on a "shoal", may attain force levels exceeding 250 MN. Forces at such magnitude are significant compared to the ships displacement, and will interfere with the ships hydrostatic condition. This yields new bending moments, which may have a significant influence on the grounding process.

6.1. Global bending moment due to grounding actions

A tanker's water plane is fairly regular. Bending moments caused by stranding and changes in water level, can therefore be found from linear considerations. A simple computer program is applied for this purpose. By applying a unit load of 1 MN at various locations, a bending moment envelope curve is made. The influence lines plotted in Fig. 16 shows that grounding amidship yields the largest global bending moment. According to DnV rules, the minimum midship stillwater hogging moment requirement for this ship is

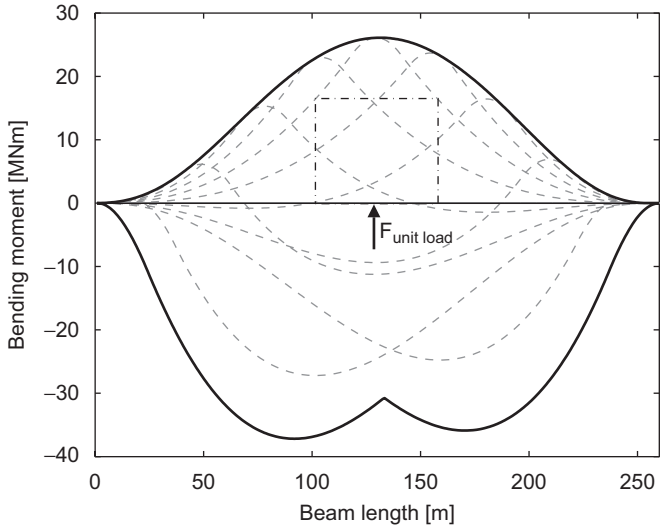

Fig. 16. Envelope bending moments with influence lines. Calculated from unit loads of 1 MN.

4100 MNm. In Fig. 13, forces are observed to reach a values greater than 250 MN. Consulting Fig. 16 this yields a hogging moment close to 6500 MNm. Clearly, the subsequent bending moments are substantial. At such magnitude there may be interaction with contact forces and stresses from global hogging.

The unit load–bending moment relation, given in Fig. 16, may be integrated in the FE simulations. It is assumed that the FE model on the global scale will behave predominantly as a rigid body. Furthermore, it is assumed that grounding amidship induces heave motions only. Bending effects are applied to the boundaries of the FE model as functions of the contact force. These functions can either be found from the unit load influence lines in Fig. 16, or by the analytical expression in Eq. (3)

$$M_b = M_0 + \frac{F_c}{A_w}\int_0^{l/2-x_b} \tilde{x}\,\mathrm{d}A_w = M_0 + 16F_c, \tag{3}$$

where F_c is the contact force, A_w the total water plane area, and M_0 the initial stillwater bending moment. $\tilde{x}$ is a local coordinate, located at the boundary of the FE model, in the global midship $x-z$ system. x_b denotes the half length of the FE model, Fig. 17. The water plane stiffness is found from numerical integration of the water lines. This is based on a simple curve fit of the bow and stern water line, which are assumed identical. Eq. (3) is valid until the hull starts to break up, as illustrated in Fig. 17.

6.2. Damage of a flexible ship

When the combination of grounding forces and global hogging attains the ultimate resistance of the girder, the fore and aft part of the hull girder start to rotate like rigid bodies, as illustrated in Fig. 17. This causes immersion of the bow and stern into the water, which may to some extent relax the hogging moment. Global force equilibrium can be found from the heave motion, z, and the rotation, θ, of the hull girder, by the expression

$$F_c = 2\rho g\left[\frac{1}{2}A_w z - \theta\int_0^{l/2} x\,\mathrm{d}A_w\right]. \tag{4}$$

The equivalent bending moment at the boundary of the model is given by

$$M_b = M_0 + \rho g\left[z\int_0^{l/2-x_b} \tilde{x}\,\mathrm{d}A_w - \theta\int_0^{l/2-x_b} \tilde{x}(\tilde{x}+x_b)\,\mathrm{d}A_w\right]. \tag{5}$$

By combining Eqs. (4) and (5), the following linear relation between contact force, hull rotation, and global bending moment is obtained:

$$M_b = M_0 + 16(F_c - 3.0\times 10^9\theta), \tag{6}$$

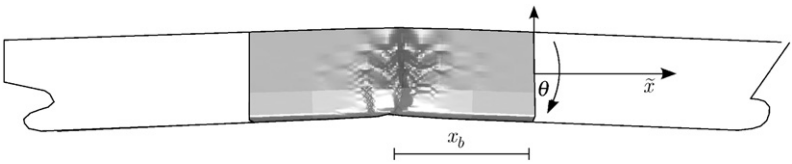

Fig. 17. Ship bending kinematics.

where units are given in (m, rad, N). This expression is implemented into LS-DYNA, which automatically reads rotations and forces and calculates the corresponding bending moment.

6.3. Grounding response

Large indenters such as the one represented by the "shoal", induce large structural damage. The forces involved are also of considerable magnitude, thus analyses with integrated hull girder bending moment interaction are made.

Four "shoal" grounding cases are analyzed. All of these simulate grounding amidship, as in "shoal scenario 3", i.e. the indenter is positioned between transverse bulkheads in the center of the ship. The interaction with global bending moments is varied as follows:

- *Case* 1: The initial bending moment is $M_0 = 4100\,\text{MNm}$. The contributions from heave and hull rotation are taken into account according to Eq. (6).
- *Case* 2: $M_0 = 0$, otherwise it is equal to case 1.
- *Case* 3: $M_0 = 4100\,\text{MNm}$, hull rotation is not taken into account, i.e. the bending moment variation due to heave is based on Eq. (3).
- *Case* 4: $M_0 = 0$, otherwise the same as case 3.

Fig. 18 shows the force history and bending moments for the four analyzed cases. The fifth dashed line is a reference curve given by "shoal" scenario 3, i.e. grounding with no global bending moments. Clearly, the global hogging moment influences the damage resistance. The curves separate after less than 1 m displacement. At this point the bottom structure is clearly affected by the large longitudinal forces from global hogging. In cases 1 and 3, the outer shell, with stiffeners start buckling although the ultimate resistance is not yet attained. The same effect is not observed in cases 2 and 4, due to far less hogging.

Collapse of the hull beam is initiated after 1.6–1.8 m displacement. It is triggered by the failure of the longitudinal center bulkhead above the inner bottom. Damage in the double bottom at this point is substantial, but the web is not yet fully crushed. Before bulkhead

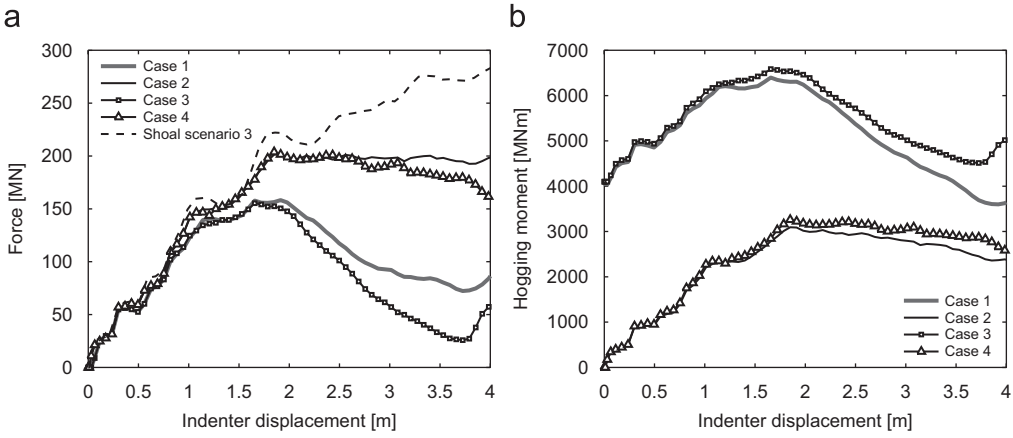

Fig. 18. Force and moment curves: (a) force–displacement curves for various hogging moments for grounding at mid tank; (b) hogging moments at the FE model boundaries.

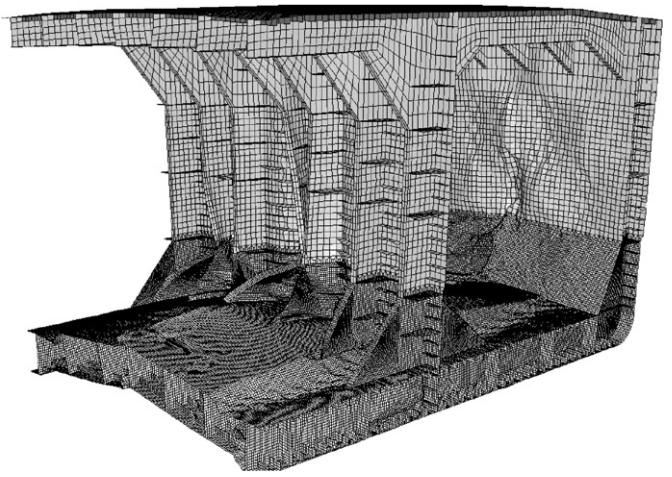

Fig. 19. Bottom structure collapse.

failure, small buckles are observed between the panel stiffeners. The bulkhead collapse is therefore a reaction of biaxial buckling, caused by force components from bending and ground contact. Fig. 19 shows the deformed ship section, with the buckled bulkhead and ship sides.

The difference between modeling the ship as a rigid, Eq. (3), versus as a "flexible" structure equation (6) is shown in Fig. 18. Prior to bulkhead collapse the difference is minimal. Introduction of the rotational component raises the resistance in the post collapse regime, because the bending moments are relaxed by immersion of the bow and stern.

The indenter displacement in Fig. 18 is not a true measure of penetration, but rather an indenter displacement within the FE analyses. After collapse, the hull beam breaks up, and the global stiffness is lost. This means that the hull will displace with the indenter in the contact area, due to rotation of both parts of the broken hull, see Fig. 17. Corrections are therefore needed. A better estimation on the "true" penetration is found by measuring the indenter displacement relative to the motions of the deck. The force penetration curves are illustrated in Fig. 20.

Fig. 21 shows the ship motion as a function of the tide, and is measured at the collapse point. The dotted line illustrates the ship displacement if no deformations are allowed, i.e. the tide and ship displacement are equal. The other two curves (black and gray) describe the total displacement and the rigid body component of Eq. (4), respectively. Clearly, the rotation component is very little in the initial state. After collapse, it becomes significant, especially in Fig. 21(a), due to the large hogging moments. Comparison with Fig. 20 (case 1) and Fig. 21 shows that loss in grounding forces results in rigid body immersion back into the water. The sinking motion of the collapse zone is, however, cancelled out by the rotation induced displacements of the broken hull. It is interesting to observe that collapse may occur after only 3–4 m variations in tide. Such variations are found at numerous locations world wide and have contributed to destruction of stranded ships. An example is the heavily damaged container vessel MSC "Napoli" which grounded south west of England in early 2007.

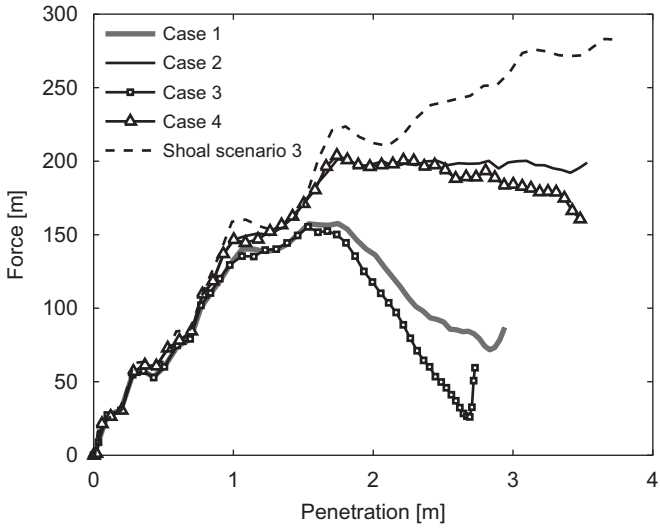

Fig. 20. Force–true penetration curves for various boundary conditions for grounding at mid tank.

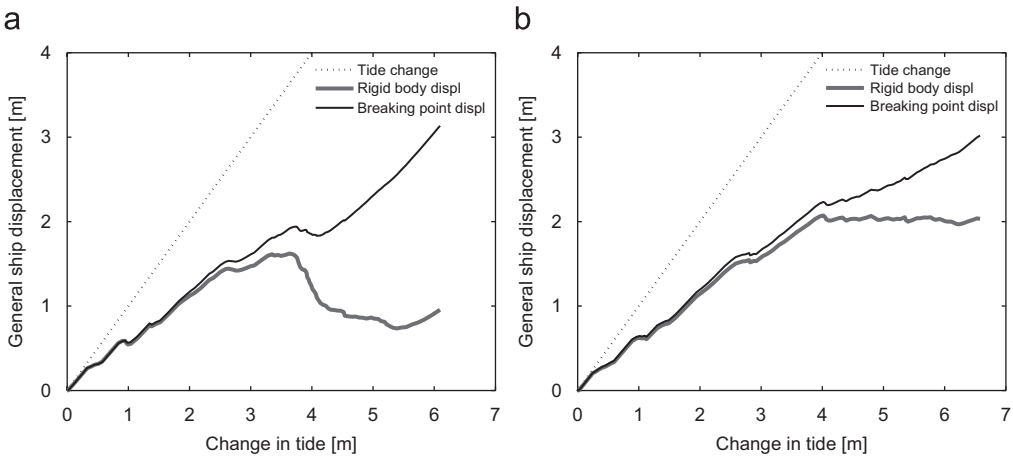

Fig. 21. Tide displacement versus mid ship displacement: (a) case 1; (b) case 2.

7. Conclusions

The paper has discussed the importance of the shape and size of sea bed topology with respect to grounding damage. A set of grounding scenarios represented by different indenters at various locations, have been analyzed. The results of the study, show that the traditional pinnacle indenter punctures the skin easily with local structural damage. Large "shoals" or dish-type indenters, on the other hand, may deform large parts of the hull structure. This may be in the form of web crushing and grillage deformation of the double bottom web. Even though, the outer hull may not fracture, the overall damage

may be severe, which in the worst case may threaten global hull bending resistance of the ship.

The interaction between the grounding actions and the hull bending moment has been studied through series of coupled FE analyses. Changes in hydrostatic conditions, as the ship is displaced out of the water, are applied onto the FE models through bending moment functions. These functions are derived directly from the hydrostatic conditions of the ship. The study shows that the coupling between the hogging moments and the contact forces affects both the longitudinal and penetration resistance of the hull. This is clearly seen as the ship is grounded and the hogging moments are increased. During the process, fracture does not take place. However, the buckling of the longitudinal sections, from global bending, and the reduced cross section, from crushing caused by the indenter, severely reduces the capacity of the hull. This finally results in the collapse of the hull beam.

Acknowledgments

The information embedded in the present paper is generated as part of the EC project Decision Support System for Ships in Degraded Condition (DDS_DC) carried our by a consortium consisting of MARINTEK (NO), BMT (UK), The Technical University of Berlin (D), The Norwegian University of Science and Technology (NO), Carnival Cruises (UK), TeeKay Norway (NO), MARTEC S.p.a. (I), Kongsberg Maritime (NO), LODIC (NO) and SIEMENS Marine Solutions (D). The financial support of the European Commission is gratefully acknowledged, as is the technical and operational contributions from Carnival and TeeKay to the use case scenario.

References

[1] Wierzbicki T, Thomas P. Closed form solution for wedge cutting force through thin metal sheets. Int J Mech Sci 1993;35:209–29.
[2] Simonsen BC, Wierzbicki T. Plasticity, fracture and friction in steady state plate cutting. Int J Impact Eng 1998;21:387–411.
[3] Simonsen BC. Ship grounding on rock I Theory. Marine Struct 1997;10:519–62.
[4] Simonsen BC. Mechanics of ship grounding. PhD thesis, DTU, 1997.
[5] Wierzbicki T. DAMAGE reports, joint mit-industry program on tanker safety. Technical report. Cambridge, MA: MIT; 1992–1999.
[6] Amdahl J, Kavlie D. Experimental and numerical simulation of double hull stranding. DNV-MIT workshop on: mechanics of ship collision and grounding, 1992.
[7] Naar H, Kujala P, Simonsen BC, Lundolphy H. Comparison of the crashworthiness of various bottom and side structures. Marine Struct 2002;15:443–60.
[8] Wang G, Arita K, Liu D. Behavior of a double hull in a variety of stranding or collision scenarios. Marine Struct 2000;13:147–87.
[9] Lützen M, Simonsen BC. Grounding damage to conventional vessels, World maritime technology conference, San Fransisco, 2003.
[10] Amdahl J, Kavlie D, Johansen A. Tanker grounding ressistance. In: PRADS 95, 1995.
[11] Zhang A, Suzuki K. Dynamic FE simulations of the effect of selected parameters on grounding test results of bottom structures. SAOS 2006;1:117–25.
[12] Hallquist J. Ls-dyna theory manual ls971. Technical report, Livemore Software, 2007.
[13] Cockcroft MG, Latham DJ. Ductility and the workability of metals. Jpn. I st Met 1968.
[14] Rice J, Tracey D. On the ductile enlargement of voids in triaxial stress fields. J Mech Phys Solids 1969;17:201–17.
[15] Törnqvist R. Design of crashworthy ship structures. PhD thesis, DTU, 2003.

[16] Törnqvist R, Simonsen BC. Experimental and numerical modelling of ductile crack propagation in large-scale shell structures. Marine Struct 2004;17:1–27.
[17] Belytschko T, Liu WK, Moran B. Nonlinear finite elements for continua and structures. LDT: Wiley: 2004.
[18] Wang G, Ji C, Kujala P, Gab Lee S, Marino A, Sirkar J, Suzuki K, Terndrup Pedersen P, Vredeveldt AW, Yuriy V. Committee v.1, collision and grounding. International Ship and Offshore Structures Congress, Southampton, UK, 2006.